

Article

Application of Kalman Filter for Estimating a Process Disturbance in a Building Space

Deuk-Woo Kim ^{1,*}  and Cheol-Soo Park ²

¹ Korea Institute of Civil Engineering and Building Technology, Goyang-si, Gyeonggi 10205, Korea

² School of Civil, Architectural Engineering and Landscape Architecture, Sungkyunkwan University, Suwon, Gyeonggi 16419, Korea; cheolspark@skku.ac.kr

* Correspondence: deukwookim@kict.re.kr; Tel.: +82-31-910-0152

Received: 17 July 2017; Accepted: 16 October 2017; Published: 18 October 2017

Abstract: This paper addresses an application of the Kalman filter for estimating a time-varying process disturbance in a building space. The process disturbance means a synthetic composite of heat gains and losses caused by internal heat sources (e.g., people, lights, equipment), and airflows. It is difficult to measure and quantify the internal heat sources and airflows due to their dynamic nature and time-lag impact on indoor environment. To address this issue, a Kalman filter estimation method was used in this study. The Kalman filtering is well suited for situations when state variables of interest cannot be measured. Based on virtual and real experiments conducted in this study, it was found that the Kalman filter can be used to estimate the time-varying process disturbance in a building space.

Keywords: Kalman filter; state augmentation; internal heat gain; uncertainty

1. Introduction

For dynamic energy simulation of existing buildings, various kinds of simulation inputs are required. Some of simulation inputs are uncertain and thus an estimation process is involved (e.g., model calibration). The uncertain variables can be classified into “static” and “dynamic”. It is relatively easy to estimate the static uncertain data because they are literally static. Examples of the static data are the thermal properties of building envelopes. In contrast, the dynamic uncertain data are time-varying and the examples of them are internal heat gains from people, lights and equipment, and heat gain/loss by airflows (infiltration, ventilation, and air movement between zones). The aforementioned dynamic data (hereafter referred to as process disturbance), are not easily quantifiable due to the following reasons:

- In most buildings, occupancy information of each space is not collected because of the privacy issue. Moreover, the sensible and latent heat gain from people vary according to age, sex, and activities [1].
- Electric consumption by lights and equipment (PCs, laptops, printers, etc.) is not generally sub-metered. Moreover, heat release from those varies depending on their types, specifications, and part load [1].
- It is difficult to measure the airflows by infiltration, ventilation, and air movement between zones) in each space [2].

Please note that the solar gains were purposefully excluded in this study. The reasons are twofold: (1) there are many advanced theories, techniques and instruments either to estimate or to measure transmitted solar gains into the room space; (2) Compared to solar gains, the authors were more

interested in estimating the uncertain dynamic internal heat gains such as infiltration, ventilation, and air movement between zones.

Incomplete information on simulation inputs leads to inaccurate simulation prediction [3,4], and causes a gap between simulation prediction and reality [5]. Various estimation techniques have been proposed so far [6]: optimization-based parameter estimation (deterministic calibration) [7], manual calibration (ad-hoc fashion, trial and error) [8], evidence-based calibration (based on the measurements of key parameters) [9], and Bayesian calibration (computationally demanding, limited to static stochastic estimation) [10]. However, the aforementioned techniques are not suitable for estimation of the process disturbance, because these are “time-varying” even in a single time horizon and thus their search space is usually vast. For example, one has to search 1440 (=24 h × 60 cases/h) cases to unknown internal heat gain at each minute in a zone for one day. For this reason, a scenario [10,11] or a profile as an estimate [8,12] are being used.

In this study, Kalman filtering, one of the state estimation algorithms, was used for estimation of the time-varying process disturbance. As mentioned above, the process disturbance means the aggregation of heat gain/loss from internal heat sources (people, lights, and equipment), and heat gain/loss by airflows (infiltration, ventilation, and air movement between zones). The Kalman filter (hereafter referred to as KF) effectively estimates unknown disturbances using existing knowledge, for example, mathematical models and a statistical property of measurement noise. Hence, the KF approach is a kind of the model-based estimation methods, and suited for a situation where measurement data are limited, but mathematical models are available. The KF has been used in many practical engineering problems; trajectory estimation (tracking aircraft, satellites, and rockets), advance controls, robotics, chemical plant operation, structural health monitoring, weather prediction, etc. [13–16].

In the field of building energy simulation, Madsen and Holst [17] showed that the KF could be applied to estimate unknown physical parameters of a building space. They developed a simplified two-time-constant model of the room, and estimated lumped parameters. The calibrated model showed good accuracy. Federspiel [18] showed an application of the KF to estimate source strength of CO₂ from occupants. The source strength, regarded as an “unknown input”, was modeled in a gas transport model. Then, the process disturbance (source strength) was estimated using a state-augmentation technique. The result showed that the KF can estimate the source strength of CO₂ from occupants and it can be used in the control of building service systems. Fux et al. [19] applied the extended KF to a dual estimation problem. With regard to a lumped thermal model of a passive house, uncertain parameters (resistance, capacitance) and disturbances (e.g., infiltration caused by occupants) were estimated.

In this study, the KF was applied to estimate the unknown process disturbance. The KF’s performance was investigated with two experiments as follows:

- Virtual experiment—a single room simulation model (3 m high, 3 m wide and 3 m deep) was made under a clear sky condition in two summer days. The time-varying aggregated heat gain/loss rate was manipulated inside the full dynamic simulation model. Four simulation cases were designed to test the KF estimation performance with regard to the heat gain/loss rate of the simulation room model.
- Mini test-bed experiment—a small-scale real experiment was conducted in a rectangular box made of expanded polystyrene. The box represents a room space and electric heating cables installed inside the box emulates a convective heating system. Two experimental cases were conducted to test the KF estimation performance of time-varying electrical heat releases from the cables.

2. Kalman Filtering

2.1. Algorithm

The KF sequentially estimates “expected” states of a stochastic dynamic system with measured data [13–16]. The “stochastic” means that a system model includes the process noises/disturbances (or modeling errors) and measurement noises. The KF calculates propagation of the estimated states as well as their uncertainty in the form of an error covariance matrix in progress of time. The propagation of the error covariance is used to check for convergence of the filter or estimation uncertainty. Finally, the KF provides unbiased estimate if statistical properties of the process noise and the measurement noise follow Gaussian distribution [13–16].

Table 1 shows the main elements of the KF. Where \mathbf{x} is a state vector of n by 1 size, \mathbf{F} is a system matrix of n by n size, \mathbf{G} is an input matrix of n by n size, \mathbf{u} is a control vector of n by 1 size, \mathbf{z} is a measurement vector of m by 1 size, \mathbf{H} is a measurement matrix of m by n size, w and v are zero-mean Gaussian white noises (n by 1 and m by 1 sizes). Noises of w and v have $N(0, \mathbf{Q})$, $N(0, \mathbf{R})$ respectively where \mathbf{Q} and \mathbf{R} are process and measurement noise matrices (n by n and m by m size). \mathbf{P} is a covariance matrix for an estimation error (n by n size). The superscript of $+$, $-$ means a posteriori estimate and a priori estimate, respectively. The superscripts -1 and T denote an inverse and a transpose of a matrix/vector respectively. The subscript k is a sequence of time, $k = 0$ is initial condition. \hat{x} is an estimate of x and $E[\cdot]$ denotes an expectation operator.

The calculation procedure of the KF is shown in Figure 1. It predicts states and covariance based on the mathematical model (*Prediction step* in Table 1 and *Step 1* in Figure 1), afterward corrects them based on the measured data (*Correction step* in Table 1 and *Step 3* in Figure 1). This is why the KF is called a prediction-correction algorithm. The theoretical details are purposefully omitted in this paper due to the lack of space but can be found in [13–16].

Table 1. Elements and expressions in the discrete-time Kalman filter.

Element	Expression
System model	$\mathbf{x}_k = \mathbf{F}_{k-1}\mathbf{x}_{k-1} + \mathbf{G}_{k-1}\mathbf{u}_{k-1} + w_{k-1}$
Measurement model	$\mathbf{z}_k = \mathbf{H}_k\mathbf{x}_k + v_k$
Noises	Process noise: $w_k \sim N(0, \mathbf{Q}_k)$ Measurement noise: $v_k \sim N(0, \mathbf{R}_k)$ * w_k and v_k are uncorrelated each other
Initial values	$\hat{\mathbf{x}}_0^+ = E[\mathbf{x}_0]$, $\mathbf{P}_0^+ = E[(\mathbf{x}_0 - \hat{\mathbf{x}}_0^+)(\mathbf{x}_0 - \hat{\mathbf{x}}_0^+)^T]$
Prediction step	a priori error covariance calculation: $\mathbf{P}_k^- = \mathbf{F}_{k-1}\mathbf{P}_{k-1}^+\mathbf{F}_{k-1}^T + \mathbf{Q}_{k-1}$ Kalman gain calculation: $\mathbf{K}_k = \mathbf{P}_k^- \mathbf{H}_k^T (\mathbf{H}_k \mathbf{P}_k^- \mathbf{H}_k^T + \mathbf{R}_k)^{-1}$ a priori state calculation: $\hat{\mathbf{x}}_k^- = \mathbf{F}_{k-1}\hat{\mathbf{x}}_{k-1}^+ + \mathbf{G}_{k-1}\mathbf{u}_{k-1} + w_{k-1}$
Correction step	a posteriori state calculation: $\hat{\mathbf{x}}_k^+ = \hat{\mathbf{x}}_k^- + \mathbf{K}_k(\mathbf{z}_k - \mathbf{H}_k\hat{\mathbf{x}}_k^-)$ a posteriori error covariance calculation: $\mathbf{P}_k^+ = \mathbf{P}_k^- - \mathbf{K}_k\mathbf{H}_k\mathbf{P}_k^-$

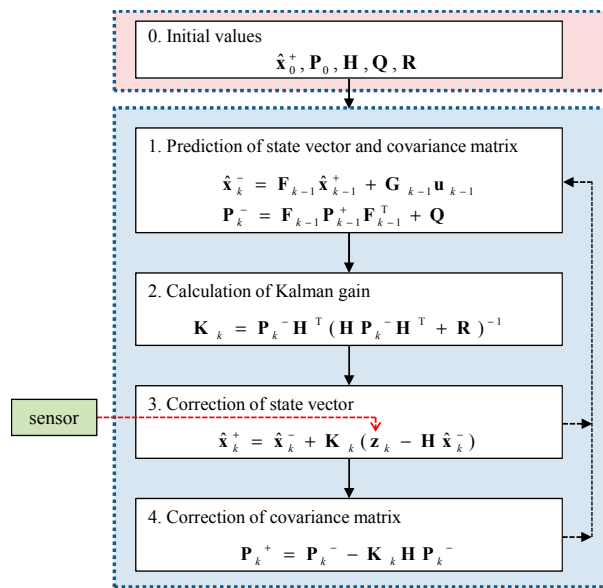


Figure 1. Overview of prediction-correction procedure of the Kalman filter.

2.2. State Augmentation

The state augmentation technique is generally used when estimating the process disturbance in the KF formulation. The unknown disturbance (\mathbf{d}) is regarded as a state variable, and added as the last element of the original state vector (\mathbf{x}). The augmented state vector \mathbf{x}' can be expressed as follows (Equation (1)):

$$\mathbf{x}'_k = \begin{bmatrix} \mathbf{x}_k \\ \mathbf{d}_k \end{bmatrix} \tag{1}$$

In general, the unknown process disturbance is assumed to follow a random walk [13–16] and its mathematical expression is as follows (Equation (2)).

$$\mathbf{d}_{k+1} = \mathbf{d}_k + w_k \tag{2}$$

where w_k is the process noise. The reason for w_k is for the KF to allow for a change in \mathbf{d}_k in progress of time. In other words, the state augmentation transforms a disturbance estimation problem into a standard form of the discrete-time KF. The augmented difference equation, driven by the noise w_k , is as follows (Equation (3)):

$$\begin{bmatrix} \mathbf{x}_{k+1} \\ \mathbf{d}_{k+1} \end{bmatrix} = \begin{bmatrix} \mathbf{F}_k & \mathbf{I} \\ 0 & \mathbf{I} \end{bmatrix} \begin{bmatrix} \mathbf{x}_k \\ \mathbf{d}_k \end{bmatrix} + \begin{bmatrix} \mathbf{G}_k \\ 0 \end{bmatrix} \mathbf{u}_k + w_k \tag{3a}$$

$$\mathbf{z}_k = \begin{bmatrix} \mathbf{H} & 0 \end{bmatrix} \begin{bmatrix} \mathbf{x}_k \\ \mathbf{d}_k \end{bmatrix} + v_k \tag{3b}$$

Equation (3a) is a discrete-time linear model, and Equation (3b) is a linear Gaussian measurement model. If only one state is measured (e.g., the first state of \mathbf{x}_k), then the measurement matrix (\mathbf{H}) will be $[1, 0, \dots, 0]$. With this augmented state vector, both \mathbf{x}_k and \mathbf{d}_k are estimated simultaneously in the prediction-correction procedure (Figure 1).

2.3. Random Walk Hypothesis for the Process Disturbance

The process disturbance is formulated as a random walk as shown in Equations (2) and (3). The random walk is a mathematical formalization of a path that consists of a succession of random steps (Equation (2)) [20,21]. The process disturbance (q_L , Equation (4)) is defined as follows:

$$q_L = q_p + q_e + q_l + q_{iv} + q_{mix} \quad (4)$$

where q_p , q_e , q_l are heat gain rate [W] from people, equipment, and lights. q_{iv} is heat gain/loss rate [W] by infiltration and ventilation [W], q_{mix} is heat gain/loss rate [W] by air movement between zones [W].

Interestingly, the aggregated process disturbance (Equation (4)) depends on the characteristics of occupant behavior [20–22]. Hence, it is difficult to describe it in a deterministic fashion. As mentioned earlier, the heat gain from people depends on their age, sex, and activities, while the heat gains from lights and equipment depend on how and when people operate those [23]. Likewise, the infiltration and ventilation depend on how and when people open/close windows/doors, and operate ventilation systems [24,25]. In addition, airflows (infiltration, ventilation, air movement between zones) in buildings are influenced by outside air temperature, wind speed and direction [26].

Rather than attempting to describe each element in the process disturbance in an analytical fashion, the authors aggregated them into a random walk fashion as shown in Equation (5):

$$q_{L,k+1} = q_{L,k} + w_k \quad (5)$$

3. Virtual Experiment

The virtual experiment provides several advantages such as accurate control of boundary conditions (e.g., indoor setpoint temperature, supply air flow rate), and capturing observable/non-observable state variables/parameters of interest. In this study, the aggregated process disturbance was generated using the EnergyPlus simulation tool, one of popular dynamic building simulation tools [27,28]. Four virtual experiments were designed to test the performance of the KF (Table 2). The case denoted as “Ref.” in Table 2 was intended to verify the estimation performance of the KF for “time-invariant” state in a building space. The case #1 was intended to verify the estimation performance under sudden changes of q_L . The case #2 was designed to verify the KF’s performance under smooth changes of q_L . With regard to the case #3, exogenous random noises were added to the generated process disturbance (q_L) of the case #2. The exogenous noises were generated by *randn* function in MATLAB [29]. An overview of four virtual experiments are as shown in Table 2 and Figure 2.

Table 2. Description of four virtual experiments.

Cases	Objective	Experiment Setting
Ref.	To test estimation performance of the KF for a time-invariant state. This can be regarded as a Reference Case.	The generated process disturbance (q_L) is set as a constant
#1	To test estimation performance of the KF under sudden changes of q_L .	The generated process disturbance (q_L) increases and decreases sharply three times a day (artificial condition).
#2	To test estimation performance of the KF under smooth changes of q_L .	The generated process disturbance (q_L) varies as a sinusoidal shape
#3	To test estimation performance of the KF under random changes of q_L . This may be close to a real-life situation in buildings (e.g., open/close windows, turn on/off lights/laptops) [20,24,25].	Random numbers were added to the generated process disturbance (q_L) of Case #2 at every 10 min

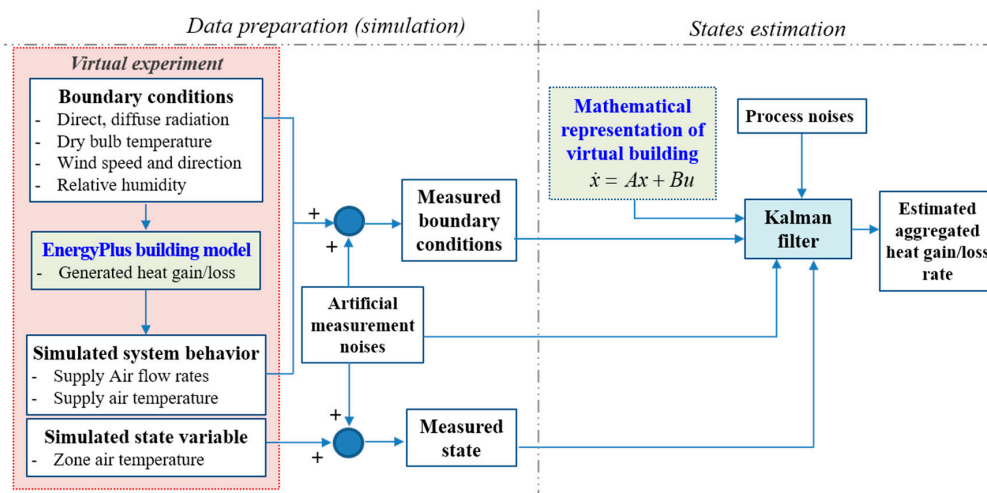


Figure 2. Overview of four virtual experiments.

3.1. Simulation Model by EnergyPlus

A simulation model was developed using EnergyPlus as shown in Figure 3. The simulated room is a rectangular office space of 3 m height, 3 m width and 3 m depth. The south facing window, 1 m by 1 m size, consists of a double glazing (6 mm clear + 12 mm air cavity + 6 mm clear). Only the south envelope has contact with outdoor environment and the others are set to be adiabatic. In this study, the medium-weight type of construction [1] was chosen. An air handling unit denoted as an ideal air system in EnergyPlus was introduced to control the room air temperature. The simulation run was conducted under a clear sky in summer.

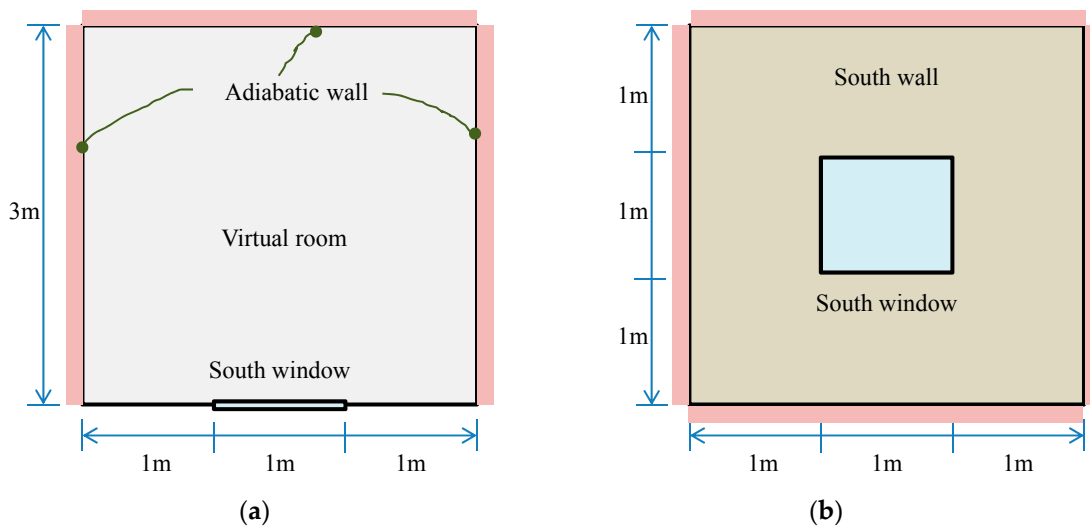


Figure 3. Simulation model: (a) Floor plan; (b) Elevation.

Artificial measurement noises (v_k) were added to the original weather data to imitate sensor noises. For this purpose, scaled random numbers were generated by MATLAB *randn* function [29] and added to the original data obtained from EnergyPlus weather data file. The list of sensors, and the magnitude of corresponding generated sensor noises are tabulated in Table 3. The weather data used for the simulation run appear in green lines as shown in Figure 4.

Table 3. List of sensors and the magnitude of their noises.

List of Sensors	Sensor Noise	Unit	Reference
Outdoor air temperature	± 0.5	($^{\circ}\text{C}$)	HOBO Weather station (H21-001)
Outdoor wind speed	± 1.2	(m/s)	Gill inc. (WindSonic 1405)
Solar radiation	± 10	(W/m^2)	LI-COR (LI-200SA)
Indoor air temperature	± 0.5	($^{\circ}\text{C}$)	General T-type thermocouple
Supply airflow speed	± 0.1	(m/s)	TESTO vane probe (0635 9335)
Supply air temperature	± 0.5	($^{\circ}\text{C}$)	General T-type thermocouple

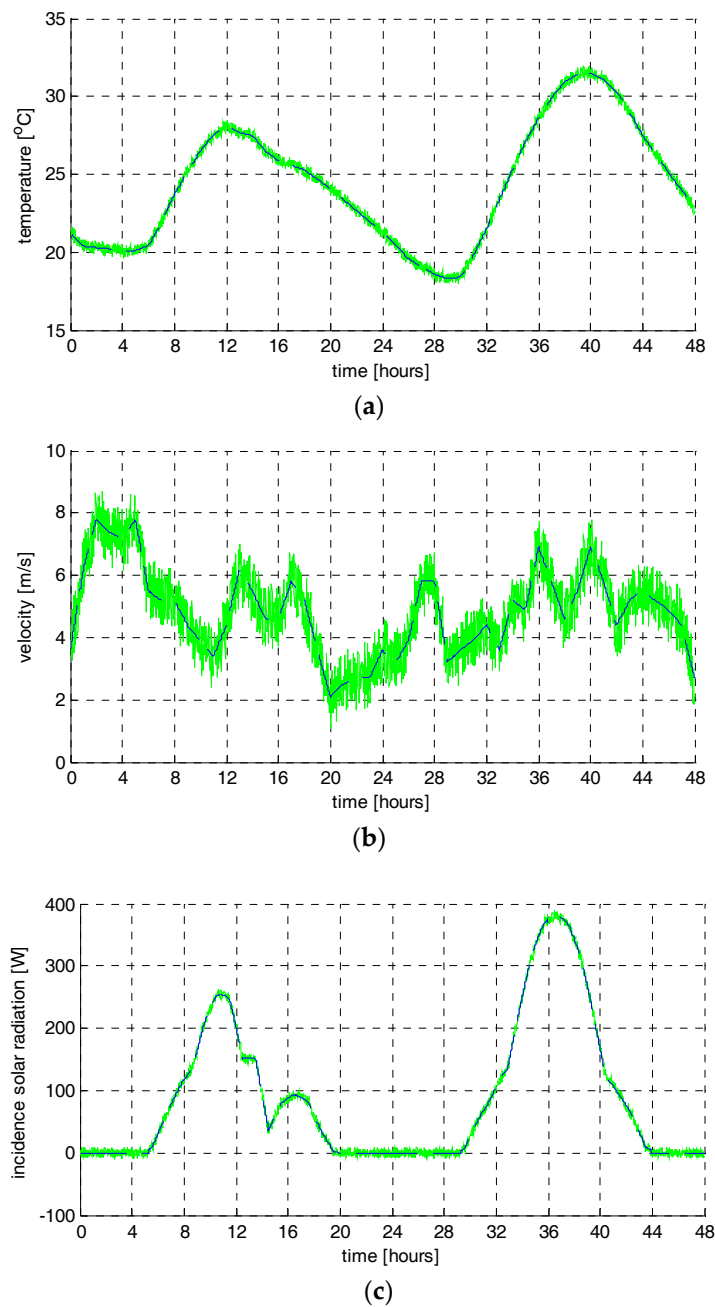


Figure 4. The original weather data (blue dotted line) and the measured weather data influenced by sensor noises (green line): (a) Outdoor air temperature; (b) Outdoor wind speed; (c) Global solar radiation incident on the south vertical wall.

3.2. Augmented State-Space Model Resembling EnergyPlus Simulation Model

The virtual building (Figure 3) was modeled as a simple resistance and capacitance network model (RC network model) as shown in Figure 5. For the sake of simplicity, a two-nodes lumped modelling approach was used for the walls, the ceiling and the floor. A one-node lumped modeling approach was applied to the south facing window based on assumption that the temperature gradient of the window in horizontal and vertical directions is negligible. Please note that this simplified RC model expressed in a state-space equation is different from the EnergyPlus simulation model (Table 4).

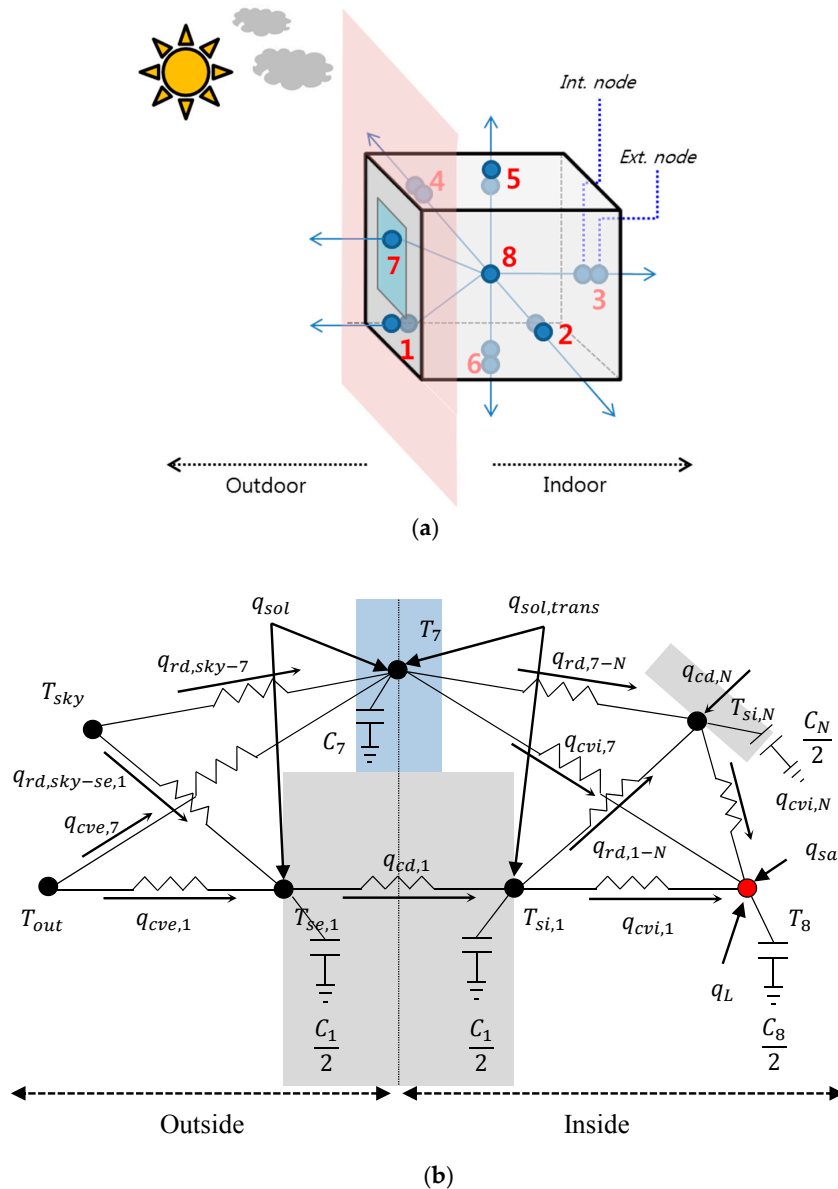


Figure 5. A state-space model of the simulation model in Figure 3: (a) Zone configuration. Each number denotes the index of the surfaces; (b) Thermal network details of the south envelope facing on the outside; T = temperature ($^{\circ}\text{C}$), C = capacity (J/K), q_L = aggregated heat gain/loss rate (W); subscript: *sky* = sky or ground, *si* = inside surface, *se* = exterior surface, N = index (1–7) of the surfaces in Figure 5a, *sa* = supply air, L = aggregated internal load, *sol* = solar radiation incident on exterior surfaces (W), *sol,trans* = transmitted solar radiation incident on interior surfaces (W), *cvi* = convection on an interior surface, *cve* = convection on an exterior surface, *rd, a – b* = radiative heat exchange between a and b surfaces, *cd* = conduction.

Table 4. Comparison of the heat transfer algorithms in the state-space model and EnergyPlus model.

Heat Transfer	State-Space Model	EnergyPlus
Wall cond.	ConductionFiniteDifference:simplified [28]	ConductionFiniteDifference [28]
Wall conv. (inside)	ASHRAE model [1]	FohannoPolidoriVerticalWall [30]
Wall conv. (outside)	SimpleCombined model [28]	MoWiTT [31]
Ceiling conv.	ASHRAE model [1]	AlamdariHammondStableHorizontal [32]
Floor conv.	ASHRAE model [1]	AlamdariHammondUnstableHorizontal [32]
Window conv. (inside)	ASHRAE model [1]	ISO15099Windows [33]
Window conv. (outside)	SimpleCombined model [28]	NaturalASHRAEVerticalWall [1]
Transmitted direct solar	All beam solar radiation entering the zone is assumed to be diffused on all surfaces	FullInteriorAndExterior: beam radiation reaches each surface in the zone by projecting the sun's rays through the exterior windows.
Long-wave heat exchange (inside)	Surface radiosity balance equation	A grey interchange model based on the ScriptF [28]

The total number of the RC network nodes is 14 including interior and exterior sides of the walls, the ceiling, and the floor, and the zone air. The order of the states in the RC model (Figure 5) is as follows.

- The 1st to 8th states represent the interior and exterior surface nodes of the walls (the surface numbers from #1 to #4 in Figure 5a)
- The 9th to 12th states represent the interior and exterior surface nodes of the ceiling and the floor (the surface numbers from #5 to #6 in Figure 5a)
- The 13th state is the window node (the window is assumed to be one node)
- The 14th state is the zone air node

The heat balance equations for the walls/ceiling/floor formulated in 1st to 12th states and the window (13th state) account for heat gains and losses by convection, conduction, and short/long-wave radiations Equation (6a–c). The heat balance equations for the surfaces #2–#6 in Figure 5a are omitted because their equations are similar to Equation (6a–c). In addition, the details of the heat transfer algorithms accounting for convection, radiation, and conduction at each inside surface #2–#6 in Figure 5a are also omitted for the same reason mentioned above. The zone air heat balance equation (Equation (6e)) for the 14th state (Equation (6d)) consists of heat gain/loss from the south façade, heat injection and removal by the air handling unit (q_{sa}), and the aggregated process disturbance (q_L). The “original” equations (Equation (6a–d)) and an “additional” equation (Equation (6e)) are combined as a state augmentation method as described in Section 2.2.

$$\frac{dT_{se,1}}{dt} = \frac{1}{C_{se,1}} (q_{cve,1} + q_{rd,1-sky} + q_{cd,1} + q_{sol,se,1}) \quad (6a)$$

$$\frac{dT_{si,1}}{dt} = \frac{1}{C_{si,1}} (q_{cvi,1} + \sum_{N=1}^7 q_{rd,si,1-si,N} + q_{cd,1} + q_{sol,trans} A_1 / \sum_{N=1}^7 A_N) \quad (6b)$$

$$\frac{dT_7}{dt} = \frac{1}{C_7} (q_{cve,7} + q_{cvi,7} + q_{rd,7-sky} + \sum_{N=1}^7 q_{rd,7-si,N} + q_{sol,trans} A_7 / \sum_{N=1}^7 A_N) \quad (6c)$$

$$\frac{dT_8}{dt} = \frac{1}{C_8} (\sum_{N=1}^7 q_{cv,si,N} + q_{sa} + q_L) \quad (6d)$$

$$\frac{dq_L}{dt} = 0 \quad (6e)$$

where each denominator C is the heat capacity (J/K) of the corresponding node, A_N is the surface area of surface N (m²) in Figure 5a.

Equation (6) is a continuous-time augmented state-space equation, and it was discretized with a sampling time of 60 s. The discrete-time KF (Table 1) is as follows (Equation (7)).

$$\mathbf{x}_{k+1} = \mathbf{F}_k \mathbf{x}_k + \mathbf{G}_k \mathbf{u}_k \quad (7)$$

It was assumed that only zone air temperature can be measured and thus the measurement matrix (\mathbf{H} ; Equation (3b)) becomes [0, 0, 0, 0, 0, 0, 0, 0, 0, 0, 0, 0, 0, 0, 1, 0].

The initial conditions for the state vector, the covariance matrix, the process noise, and measurement noises of the KF are important. For example, the magnitudes of the process noise (w_k) and the measurement noise (v_k) should be carefully determined because they influence the convergence/divergence of the Kalman filter. The conditions used in this study are tabulated in Table 5.

Table 5. Initial conditions for the virtual experiment.

Parameter	Symbol *	Value	Unit	Remark	
State vector	Wall int./ext. temperature ($i = 1, \dots, 12$)	$\mathbf{x}_{(i,1)}$	25	(°C)	Close to room air temperature
	Window temperature	$\mathbf{x}_{(13,1)}$	25	(°C)	Close to room air temperature
	Zone air temperature	$\mathbf{x}_{(14,1)}$	25	(°C)	Room air temperature set point
	Aggregated heat gain/loss rate	$\mathbf{x}_{(15,1)}$	0	(W)	No heat input at initial stage
Initial error covariance matrix	$\mathbf{P}_{(j,j)}$ ($j = 1, \dots, 14$)	$(\pm 2)^2$	(°C ²)	A confidence range would be ± 2 °C of the initial temperatures.	
	$\mathbf{P}_{(15,15)}$	$(\pm 439 \times 10\%)^2$	(W ²)	A confidence range would be $\pm 10\%$ of normal condition (439 Watt); Heat releases of people, lights, and equipment are assumed to be 10 W/m ² , 10.8 W/m ² , and 125 W/person * 2 persons respectively. The floor area is 9 m ² .	
Measurement matrix	$\mathbf{H}_{(1,14)}$	1	(-)	Only zone air temperature was measured. Hence the measurement matrix is [0, 0, 0, 0, 0, 0, 0, 0, 0, 0, 0, 0, 0, 0, 1, 0].	
	$\mathbf{H}_{(1,n)}$ ($n = 1, \dots, 13, 15$)	0	(-)		
Process noise covariance matrix	$\mathbf{Q}_{(m,m)}$ ($m = 1, \dots, 14$)	$(\pm 0.2)^2$	(°C ²)	The process noise of temperatures would be ± 0.2 °C.	
	$\mathbf{Q}_{(15,15)}$	$(\pm 439 \times 10\%)^2$	(W ²)	The estimate of the aggregated heat gain/loss rate can vary $\pm 10\%$ of 439 Watt per one minute.	
Measurement noise covariance matrix	$\mathbf{R}_{(1,1)}$	$(\pm 2)^2$	(°C ²)	The measurement noise of the zone air temperature would be ± 2 °C.	

* The numbers in subscript parenthesis represents the numbers of rows and columns in a vector or a matrix.

3.3. Results

Figure 6 shows the aggregated process disturbance in EnergyPlus (in green) and the estimated process disturbance (in blue) with 95% confidence bounds (red dotted lines). For the reference case (Table 2), the estimated value closely follows the true value of 500 Watt as shown in Figure 6a. In spite of the poor estimation at the initial stage, but the KF tracks the true value well after 1 hour and it keeps near the true value (500 Watt) for the remainder of the day. Likewise, in the case of the experiment case #1, the estimate tracks the suddenly-changed pattern similarly (Figure 6b).

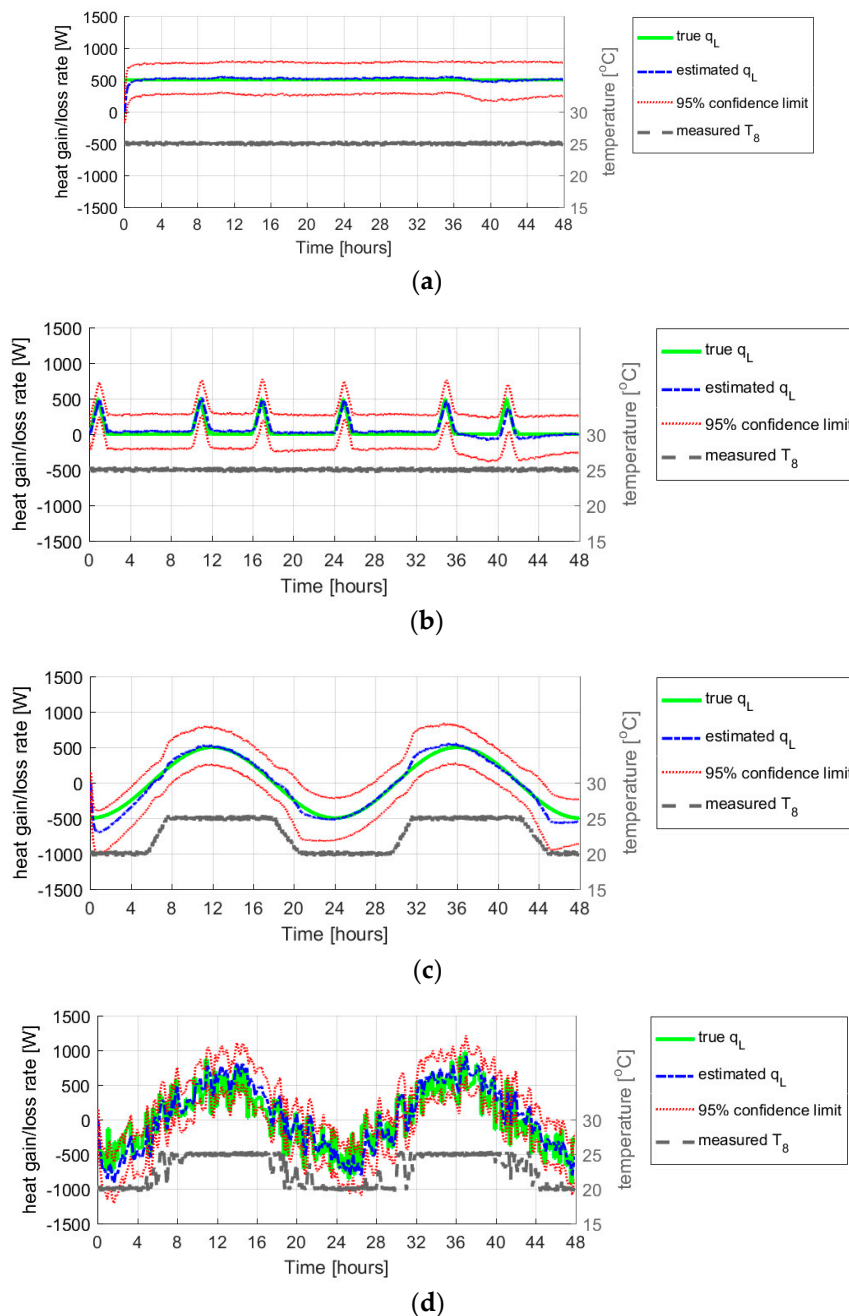


Figure 6. Comparison between the true and the estimated values (green line: true value, blue dashed line: estimate value). (a) Reference case; (b) Case #1; (c) Case #2; (d) Case #3.

In the case of the experiment case #2, likewise the KF tracks well the true value of a sinusoidal shape (Figure 6c). However, when the heating and cooling set point temperatures are changed to 20 °C or 25 °C (near 0, 20, 32, 44 h), the KF overestimates or underestimates the true value

In case #3, the random heat gains/losses were added to the generated process disturbance of case #2 at every 10 min. The true value quickly varies due to the exogenous random disturbance (Figure 6d). This is the most complicated situation but the result seems interesting.

Although a certain amount of errors exists during the day and the KF seems not to swiftly respond to the true value, the estimated confidence intervals still cover the true value. It can be concluded that the KF performs satisfactorily under the noisy disturbance condition.

For quantitative assessment, RMSE (root-mean-square error), NRMSE (normalized root-mean-square error), and R-square (coefficient of determination) were calculated (Table 6). Please note that the NRMSE and R-square values (Table 6) for the reference case are ∞ and $-\infty$ because the denominators of them are zero. For the reference case, RMSE is slightly greater by 37.9 W than the true value (500 Watt), but the discrepancy seems allowable. The cases #1–#3, NRMSEs are about 12.1%, 6.4%, and 11.8% respectively, and R-squares are 0.75, 0.97, and 0.71 respectively. The overall estimation errors seem to be acceptable considering the estimation range (from -500 to 500 Watt). It is also worth noting that the estimation error is inevitable because the augmented state-space model (Equation (6), described in Section 3.2) is different from the EnergyPlus simulation model (Section 3.1).

Table 6. Comparison of estimation performance.

Case	RMSE (W)	NRMSE (%)	R-Square (-)
Ref.	37.9	∞	$-\infty$
#1	60.5	12.1	0.75
#2	64.7	6.4	0.97
#3	225.6	11.8	0.71

4. Mini Test-Bed Experiment

In order to test the KF under a real-life situation, the mini test-bed experimental set-up reported in [34] was used in this study. A brief summary of the mini test-bed (Figure 7) is as follows; it is a rectangular box which is made of Expanded Polystyrene (EPS). It contains two types of electric heating cables (nominal heating powers are 10 Watt and 30 Watt, respectively) inside the EPS box which emulates a convective heating system. Electric consumption of the heating cables was measured by a wattmeter, and indoor air and surface temperatures of the EPS box were measured by T-type thermocouples. NI Compact DAQ 9174 was used for data acquisition.

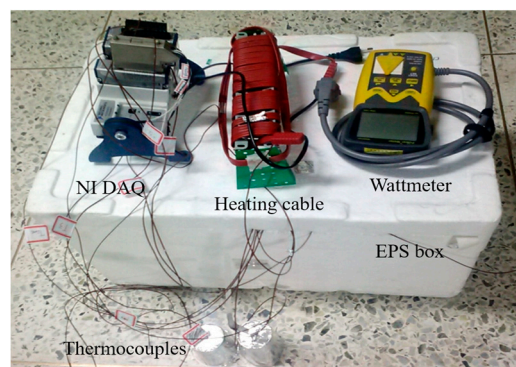


Figure 7. Configuration of the mini test-bed.

The experiment was conducted twice (28 October 2012, 29 October 2012) with the heating cables of 10 Watt and 30 Watt, which showed actual consumption power of 10.8 Watt and 26 Watt respectively. The duration of each experiment was 160 min and the sampling time was set to one second. During the experiment, two heating cables were randomly turned on/off. In this real experiment, the actual value of convective heat release rate (e.g., instantaneous gain) from the heating cable is unknown because it is not measurable. This is a significant difference between the virtual and real experiments. Therefore, the measured electric power of the heating cable was used for validation. An overall overview of the experiment procedure is shown in Figure 8.

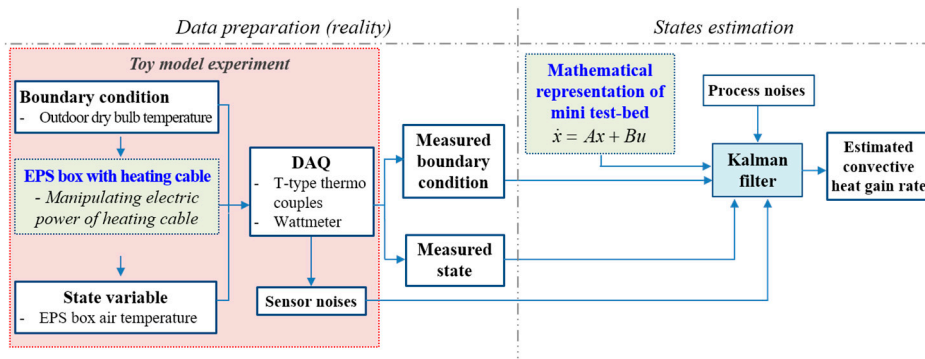


Figure 8. Overview of the mini test-bed experiment.

4.1. Augmented State Space Model of the Mini Test-Bed

The modeling approach is the same as that of the virtual experiment. The heat balance equations at each node (Figure 9) were based on [28] and the detailed explanation of it is omitted for the sake of brevity. The mini test-bed was designed with the purpose of indoor experiment; hence exterior environmental effects (wind and solar radiation, etc.) were not included. The size of the state vector is 14 due to the absence of the window node (Figure 5 vs. Figure 9). The discretization step was set to one second.

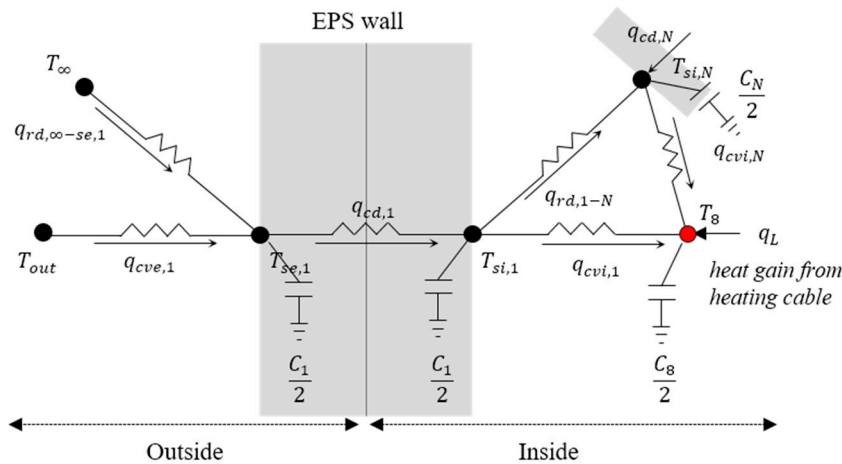


Figure 9. Thermal network of the mini test-bed.

The initial conditions were set to be equal to those of the virtual experiment (Table 5) except the following parameters. The initial error covariance (**P**) was modified to take the nominal power of the heating cable (10 Watt and 30 Watt) into account. The magnitude of the process noise matrix (**Q**) was also modified to take the discretization step size into account (one minute in the virtual experiment vs. one second in the mini test-bed experiment). The magnitude of the measurement noise matrix (**R**) was modified to take a small volume of the EPS box into account. The initial conditions are tabulated in Table 7.

Table 7. Initial conditions for the mini test-bed experiment.

Parameter	Symbol *	Value	Unit	Comments
State vector	Wall int./ext. temperature $x_{(i,1)}$ ($i = 1, \dots, 12$)	25	(°C)	Close to room air temperature
	Air temperature in the EPS box. $x_{(13,1)}$	25	(°C)	Close to room air temperature
	Heat release rate $x_{(14,1)}$	0	(W)	No heat release at initial stage
Initial error covariance matrix	$P_{(j,j)}$ ($j = 1, \dots, 13$)	$(\pm 2)^2$	(°C ²)	A confidence range would be ± 2 °C of the initial values
	$P_{(14,14)}$	$(\pm 30 \times 10\%)^2$	(W ²)	The nominal heating cable power is 30 Watt at maximum. The confidence range would be 10% of the initial value.
Measurement matrix	$H_{(1,13)}$	1	(-)	Only box air temperature is measured. Hence the measurement matrix is [0, 0, 0, 0, 0, 0, 0, 0, 0, 0, 0, 0, 0, 0, 1, 0].
	$H_{(1,m)}$ ($m = 1, \dots, 12, 14$)	0	(-)	
Process noise covariance matrix	$Q_{(m,m)}$ ($m = 1, \dots, 13$)	$(\pm 0.2)^2$	(°C ²)	The process noise of temperatures would be ± 0.2 °C.
	$Q_{(14,14)}$	$(\pm 30 \times 10\%)^2$	(W ²)	The estimate of the heat release rate can vary $\pm 1\%$ of 30 W per second.
Measurement noise covariance matrix	$R_{(1,1)}$	$(\pm 2)^2$	(°C ²)	The measurement noise would be ± 2 °C

* The numbers in subscript parenthesis represents the numbers of rows and columns in a vector or a matrix.

4.2. Results

During the experiment, the heating cables of 10 Watt and 30 Watt, were turned on and off four times, three times respectively (Figure 10). Please note that the actual consumption powers of the heating cables of 10 Watt and 30 Watt were 10.8 Watt and 26 Watt respectively (Figure 10). The reason for random ons/off is to make heat release pattern be unpredictable and then to test whether the KF can perform well under such case. As shown in Figure 10, the box air temperature slowly increases with time-lag when the heating cable is turned on. It seems that the thermal capacity of the heating cable and the box air volume delays the temperature increase.

The convective heat release from the heating cable, regarded as the process disturbance, is unknown and not measurable. Hence it was compared to the electric power consumption in green line. It is shown that the errors were roughly 3 Watt and 5 Watt deviated from the consumed power (10.8 Watt and 26 Watt) respectively during the periods (Figure 10).

The estimation performance for tracking the heat release (q_L) can be judged by comparing (q_L to the measured box air temperature. Both of q_L and T_8 are similar to each other. It can be concluded that the heat releases by the cables are reasonably estimated by the KF.

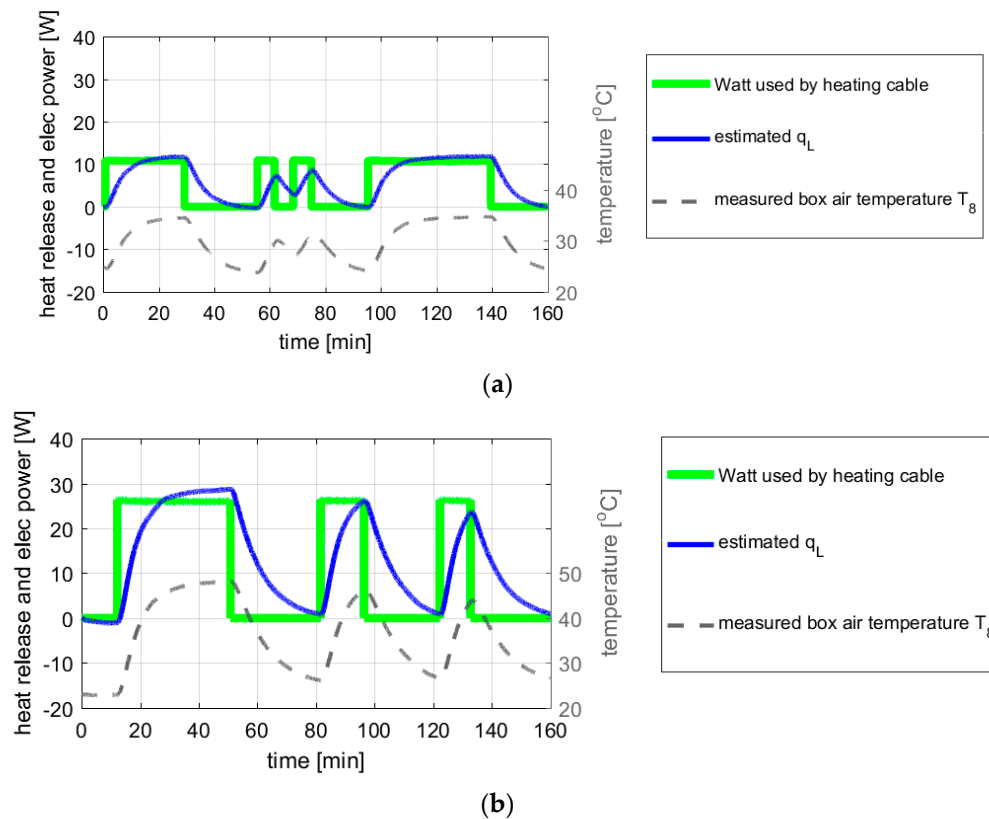


Figure 10. Comparison between the electric power of the heating cable (the true value, in green line) and the estimated heat release rate (q_L , in blue line) and with the 95% confidence limits (red dotted lines). The measured box air temperature (T_8 , dashed grey line) is plotted together: (a) when 10 Watt heating cable was used (measured value is 10.8 Watt); (b) when 30 Watt heating cable was used (measured value is 26 Watt).

5. Conclusions

This paper addressed the estimation performance of the KF for the aggregated process disturbance (the sum of heat gains and losses from internal sources). The virtual experiment and the real experiment were conducted. According to the results, it can be concluded that reliable estimation of unknown simulation inputs can be made using the KF method.

In the case of the virtual experiments (Ref., Cases #1, #2, and #3), it was shown that the KF can estimate the time-invariant and time-varying process disturbances. The overall estimation errors of NRMSE were about 6.4–12.1%. During the real mini test-bed experiment, the convective and radiative heat release rates from the heating cable are not measurable. Therefore, the electric power consumption of the heating cable was used as a substitute for validation. The result showed that the estimation errors range from 3 Watt to 5 Watt, deviating from the real values (10.8 Watt and 26 Watt) during the steady-state period.

Acknowledgments: This research was supported by a grant (17AUDP-B079104-04) from Architecture & Urban Development Research Program funded by Ministry of Land, Infrastructure and Transport of Korean government.

Author Contributions: Deuk-Woo Kim implemented the Kalman filtering and two experiments. Deuk-Woo Kim and Cheol-Soo Park analyzed the results together.

Conflicts of Interest: The authors declare no conflict of interest.

References

1. American Society of Heating, Refrigerating and Air-Conditioning Engineers (ASHRAE). *ASHRAE Handbook of Fundamentals*; American Society of Heating, Refrigerating and Air-Conditioning Engineers, Inc.: Atlanta, GA, USA, 2013.
2. McWilliams, J. *Review of Airflow Measurement Techniques*; LBNL-49747; Lawrence Berkeley National Laboratory: Berkeley, CA, USA, 2002.
3. Hopfe, C.J.; Hensen, J.L.M. Uncertainty analysis in building performance simulation for design support. *Energy Build.* **2011**, *43*, 2798–2805. [[CrossRef](#)]
4. Ahn, K.U.; Kim, D.W.; Kim, Y.J.; Yoon, S.H.; Park, C.S. Issues to Be Solved for Energy Simulation of An Existing Office Building. *Sustainability* **2016**, *8*, 345. [[CrossRef](#)]
5. De Wilde, P. The gap between predicted and measured energy performance of buildings: A framework for investigation. *Autom. Constr.* **2014**, *41*, 40–49. [[CrossRef](#)]
6. Reddy, A.T. Literature review on calibration of building energy simulation programs: Uses, problems, procedures, uncertainty, and tools. *ASHRAE Trans.* **2006**, *112*, 226–240.
7. Reddy, T.A.; Maor, I.; Panjapornpon, C. Calibrating Detailed Building Energy Simulation Programs with Measured Data Part II: Application to Three Case Study Office Buildings. *HVAC R Res.* **2007**, *13*, 243–265.
8. Liu, G.; Liu, M. A rapid calibration procedure and case study for simplified simulation models of commonly used HVAC systems. *Build. Environ.* **2011**, *46*, 409–420. [[CrossRef](#)]
9. Raftery, P.; Keane, M.; Costa, A. Calibrating whole building energy models: Detailed case study hourly measured data. *Energy Build.* **2011**, *43*, 3666–3679. [[CrossRef](#)]
10. Heo, Y.S.; Choudhary, R.; Augenbroe, G.A. Calibration of building energy models for retrofit analysis under uncertainty. *Energy Build.* **2012**, *47*, 550–560. [[CrossRef](#)]
11. American Society of Heating, Refrigerating and Air-Conditioning Engineers (ASHRAE). *90.1 User's Manual*; ANSI/ASHRAE/IESNA Standard 90.1-2004; American Society of Heating, Refrigerating and Air-Conditioning Engineers, Inc.: Atlanta, GA, USA, 2004.
12. Carling, P.; Isakson, P.; Blomberg, P.; Eriksson, J. *Experiences from Evaluation of the HVAC Performance in the Katsan Building Based on Calibrated Whole-Building Simulation and Extensive Trending*; A40-D-M6-SWE-AF/KTH-2; IEA Annex 40 Working Paper; IEA: Paris, France, 2003.
13. Gelb, A. *Applied Optimal Estimation*; MIT Press: Cambridge MA, USA, 1974.
14. Simon, D. *Optimal State Estimation: Kalman, H Infinity, and Nonlinear Approaches*; John Wiley & Sons: Hoboken, NJ, USA, 2006.
15. Grewal, M.S.; Andrews, A.P. *Kalman Filtering: Theory and Practice Using MATLAB*, 2nd ed.; John Wiley & Sons, Inc.: Hoboken, NJ, USA, 2001.
16. Crassidis, J.L.; Junkins, J.L. *Optimal Estimation of Dynamic Systems*, 2nd ed.; CRC Press: Boca Raton, FL, USA, 2011.
17. Madsen, H.; Holst, J. Estimation of continuous-time models for the heat dynamics of a building. *Energy Build.* **1995**, *22*, 67–79. [[CrossRef](#)]
18. Federspiel, C.C. Estimating the inputs of gas transport processes in buildings. *IEEE Trans. Control Syst. Technol.* **1997**, *5*, 480–489. [[CrossRef](#)]
19. Fux, S.F.; Ashouri, A.; Benz, M.J.; Guzzella, L. EKF based self-adaptive thermal model for a passive house. *Energy Build.* **2014**, *68*, 811–817. [[CrossRef](#)]
20. Ahn, K.U.; Park, C.S. Correlation between occupants and energy consumption. *Energy Build.* **2016**, *116*, 420–433. [[CrossRef](#)]
21. Ahn, K.U.; Kim, D.W.; Park, C.S.; de Wilde, P. Predictability of occupant presence and performance gap in building energy simulation. *Appl. Energy* **2017**, in press. [[CrossRef](#)]
22. Yan, D.; O'Brien, W.; Hong, T.; Feng, X.; Gunay, H.B.; Tahmasebi, F.; Mahdavi, A. Occupant behavior modeling for building performance simulation: Current state and future challenges. *Energy Build.* **2015**, *107*, 264–278. [[CrossRef](#)]
23. Duska, M.; Lukes, J.; Bartak, M.; Drkal, F.; Hensen, J.L.M. Trend in heat gains from office equipment. In Proceedings of the 6th International Conference on Indoor Climate of Buildings, Bratislava, Slovakia, 28 November–1 December 2007.

24. Pierce, J.; Schiano, D.J.; Paulos, E. Home, habits, and energy: Examining domestic interactions and energy consumption. In Proceedings of the CHI 2010: Home Eco Behavior, Atlanta, GA, USA, 10–15 April 2010; pp. 1985–1994.
25. Andrews, C.J.; Yi, D.; Krogmann, U.; Senick, J.A.; Wener, R.E. Designing buildings for real occupants: An agent-based approach. *IEEE Trans. Syst. Man Cybern. Part A Syst. Hum.* **2011**, *41*, 1077–1091. [[CrossRef](#)]
26. De Wit, M.S.; Augenbroe, G.L.M. Analysis of uncertainty in building design evaluation. *Energy Build.* **2002**, *34*, 951–958. [[CrossRef](#)]
27. Crawley, D.B.; Lawrie, L.K.; Winkelmann, F.C.; Buhl, W.F.; Erdem, A.E.; Pedersen, C.O.; Liesen, R.J.; Fisher, D.E. What Next for Building Energy Simulation—A Glimpse of the Future. In Proceedings of the Building Simulation '97, Prague, Czech Republic, 7–10 September 1997; pp. 395–402.
28. U.S. Department of Energy (DOE). *S. Department of Energy (DOE). EnergyPlus 7.0 Engineering Reference: The Reference to EnergyPlus Calculations*; U.S. Department of Energy: Washington, DC, USA, 2011.
29. Mathworks. *Statistics Toolbox™ User's Guide, R2013a*; MathWorks, Inc.: Natick, MA, USA, 2013.
30. Fohanno, S.; Polidori, G. Modelling of natural convective heat transfer at an internal surface. *Energy Build.* **2006**, *38*, 548–553. [[CrossRef](#)]
31. Yazdani, M.; Klems, J.H. Measurement of the exterior convective film coefficient for windows in low-rise buildings. *ASHRAE Trans.* **1994**, *100*, 1087–1096.
32. Alamdari, F.; Hammond, G.P. Improved data correlations for buoyancy-driven convection in rooms. *Build. Serv. Eng. Res. Technol.* **1983**, *4*, 106–112. [[CrossRef](#)]
33. International Standardization Organization. *ISO15099—Thermal Performance of Windows, Doors, and Shading Devices—Detailed Calculations*, 1st ed.; International Standardization Organization: Geneva, Switzerland, 2003.
34. Kim, D.W.; Suh, W.J.; Jung, J.T.; Yoon, S.H.; Park, C.S. A mini test-bed for modeling, simulation and calibration. In Proceedings of the Second International Conference on Building Energy and Environment, Boulder, CO, USA, 1–4 August 2012; pp. 1145–1152.



© 2017 by the authors. Licensee MDPI, Basel, Switzerland. This article is an open access article distributed under the terms and conditions of the Creative Commons Attribution (CC BY) license (<http://creativecommons.org/licenses/by/4.0/>).